DOI 10.5162/Ultrasonic2025/C6-b3

A Holo-array for Enhancement of Ultrasonic Focusing

Yanfeng Lang[1,2], *Zhibo Yang*[1*], *Xuefeng Chen*[1], *and Zhongqing Su*[2**]
[1] *Xi'an Jiaotong University, Xian, China*
[2] *The Hong Kong Polytechnic University, Hong Kong, China, Hong Kong*
**phdapple@mail.xjtu.edu.cn **zhongqing.su@polyu.edu.hk*

Abstract: Conventional phased arrays are typically used to steer the main lobe under spatial Nyquist constraints. When these constraints are violated, grating lobes emerge. However, in Lamb-wave-based damage identification, side and grating lobes are often overlooked. To address this, a holo-array is proposed in this study. Instead of relying solely on phase control, the phase, frequency, and amplitude of the probe wave are individually tailored for each array element to steer the main lobe, suppress grating lobes, and reduce side lobes. The effectiveness is validated through experiments on an aluminum plate.

Keywords: grating lobe, side lobe, phased array, damage detection,pseudo damage

Introduction

The guided-wave-based phased array (P-array) is a highly effective technique for structural damage detection. Lamb waves, a class of guided waves propagating in plate-like structures, offer distinct advantages such as low attenuation over long distances, rapid propagation velocity, and high sensitivity to various types of damage.

However, the P-array is subject to inherent limitations in its parameter configuration. As reported by Yu et al. [1], with the increase of ratio of element pitch and wavelength of the excitation d/λ, although the beam width is narrower and narrower, which means that the direction precision is improved, more and more sidelobes (with the magnitude lower than the main lobe), even grating lobes (with the magnitude equivalent to the main lobe) appear.

To address this challenge, Antonik [2] introduced the frequency diverse array, which enables dynamic manipulation of the beam pattern in radar systems. In addition to phase and frequency, amplitude serves as a critical parameter in defining signal waveforms and controlling energy distribution within the array.

This study introduces a holo-array approach that leverages the unique dispersive property of Lamb waves. By individually customizing the phase, frequency, and amplitude of the anti-dispersive probe signal for each array element, the holo-array achieves main lobe steering, grating lobe suppression, and sidelobe reduction. The proposed method is experimentally validated on an aluminum plate.

Concept of Holo-array

In the conventional phased array composed of M elements, distinct phase delays are applied to each element to ensure that the emitted signals constructively interfere and become in-phase at the desired focal location. The phase vector can be denoted by $\boldsymbol{\varphi} = [\varphi_1, \varphi_i, ..., \varphi_M]$.

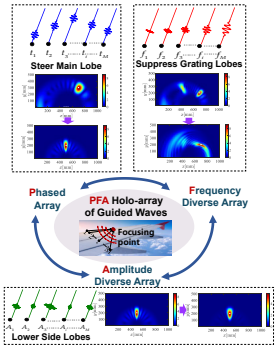

Fig. 1: The concept of PFA holo-array of ultrasonic guided waves

An emitted signal is fundamentally characterized by three parameters: amplitude, frequency, and phase. While conventional phased arrays primarily utilize phase control to achieve constructive interference at a target location, the amplitude and frequency of the array signals can also be tailored to further enhance array performance. The corresponding amplitude vector and frequency vector are denoted by $\boldsymbol{a} = [a_1, a_i, ..., a_M]$ and $\boldsymbol{f} = [f_1, f_i, ..., f_M]$.

With the objective of enhancing array energy at the desired focal point $F(x_0, y_0)$, the phase, frequency, and amplitude of the excitation signals are individually customized according to the following strategy.

The phase for the ith element is calculated by:

$$\varphi_i = k(\omega) r_i^F \tag{1}$$

where r_i^F represents the propagation distance from the ith element to the focusing point $F(x_0, y_0)$

The increasing frequency vector is designed in the work and the frequency for ith element can be calcu-

late by:

$$f_i = f_c + (i - \frac{(M-1)}{2} - 1)\Delta f \tag{2}$$

where f_c is the center frequency and Δf is frequency offset.

The Dolph–Chebyshev synthesis is adopted to construct the array pattern with equiripple sidelobes—i.e., sidelobes of equal amplitude. The amplitude a_i for the ith element of the even-element array and odd-element array can be calculated by Eq. (4) and Eq. (6), respectively.

$$\text{even:} a_i = \sum_{q=i}^{M} (-1)^{M-q} (x_0)^{2q-1} \cdot A \tag{3}$$

$$A = \frac{(q+M-2)!(2M-1)}{(q-i)!(q+i-1)!(M-q)!} \tag{4}$$

$$\text{odd:} a_i = \sum_{q=i}^{M} (-1)^{M-q+1} (x_0)^{2(q-1)} \cdot B \tag{5}$$

$$B = \frac{(q+M-2)!2M}{(q-i)!(q+i-2)!(M-q+1)!} \tag{6}$$

where $x_0 = cosh\left(\frac{cosh^{-1}(10^{-L_s/20})}{M-1}\right)$. L_s is the sidelobe level.

In this study, both amplitude and frequency are incorporated into the array control strategy. Accordingly, we propose a classification scheme for various array configurations. The conventional phased array, in which only phase control is applied, is denoted as the P-array. Arrays that incorporate both phase and amplitude control are referred to as PA-arrays, while those utilizing phase and frequency control are termed PF-arrays. The array configuration that simultaneously manipulates all three parameters is designated as the PFA holo-array.

Anti-dispersion Focusing Strategy

The tone burst signal is commonly-used for Lamb-wave-based damage detection, as shown in Eq. (7).

$$s(t) = w(t)sin(2\pi f_c t) \tag{7}$$

where $w(t)$ denotes the Hann window, which can be expressed as $w(t) = 0.5(H(t) - H(t - \frac{N_c}{f_c}))(1 - cos(\frac{2\pi f_c t}{N_c}))$. $H(\cdot)$ is the Heaviside function .Two parameters need to be determined: the number of cycles N_c and the center frequency f_c.

Lamb waves exhibit dispersive propagation characteristics. The dispersive response under the tone burst excitation at a travailing distance of r can be expressed as:

$$u^{dis}(r,t) = \mathcal{F}^{-1}(S(\omega)\mathrm{e}^{-\mathrm{j}k(\omega)r}) \tag{8}$$

where $\mathcal{F}^{-1}(\cdot)$ represents the inverse Fourier transform; $S(\omega)$ is frequency-domain of the tone burst excitation $s(t)$. Eq. (8) demonstrates that the propagated signal comprises components of varying frequencies, each experiencing a distinct phase shift of $\mathrm{e}^{-\mathrm{j}k(\omega)r}$. This frequency-dependent phase variation is the fundamental characteristic of dispersion.

The redesigned excitation for the ith PZT and the focusing point $F(x_0, y_0)$ can be written as:

$$G_i^F(\omega) = a_i S_i(\omega; f_i)\mathrm{e}^{\mathrm{j}k(\omega)r_i^F} \tag{9}$$

where $S_i(\omega; f_i)$ is the tone burst excitation centered at f_c in frequency domain. By redesigning the excitation signal for each array element and each inspection point, the dispersion compensation strategy and the array focusing mechanism of the holo-array can be simultaneously achieved.

Under the redesigned excitation, the response signal at the inspection point (x, y) can be expressed as:

$$u_i^F(x,y) = \mathcal{F}^{-1}(G_i^F(\omega)\mathrm{e}^{-\mathrm{j}k(\omega)r_i^{xy}}) \tag{10}$$

where r_i^{xy} represents the propagation distance from the ith element to the inspection point (x, y).

Focusing Pattern under Holo-array

The focusing energy pattern of the array under the redesigned anti-dispersive tone burst excitation can be calculated by:

$$E(x,y) = \left| \sum_{i=1}^{M-1} u_i^F(x,y) + \mathrm{j}\mathcal{H}(\sum_{i=1}^{M-1} u_i^F(x,y)) \right|_{t_c}, \tag{11}$$

where $\mathcal{H}(\cdot)$ represents the Hilbert transform and t_c is the focusing moment.

In this study, the uniform linear array with the element pitch of $d = 10$ mm is explored.

Figure 2 and Figure 3 compares the energy pattern focusing at $(500, 300)$ and $(600, 250)$ with various arrays respectively. For the energy pattern of the conventional P-array in Figure 2(a,e) and Figure 3 (a,e), the side lobes always exist. The grating lobes appear at higher frequency at which the Nyquist sampling theory is not satisfied at certain focusing point, as in Figure 3 (e) with the center frequency of $f_c = 120$ kHz and focusing point at $(600, 250)$. Compared with the energy pattern of the P-array, the side lobes are suppressed in the PA-array. But the disadvantage is that the width of the main lobe is expanded, as illustrated in Figure 2(b,f) and Figure 3 (b,f).

For the energy distribution of the conventional P-array shown in Figure 2(a,e) and Figure 3(a,e), sidelobes are consistently present. At higher frequencies, grating lobes emerge due to the violation of the Nyquist sampling criterion at specific focusing points, as illustrated in Figure 3(e), where the center frequency is$f_c = 120$ kHz and the focusing point is

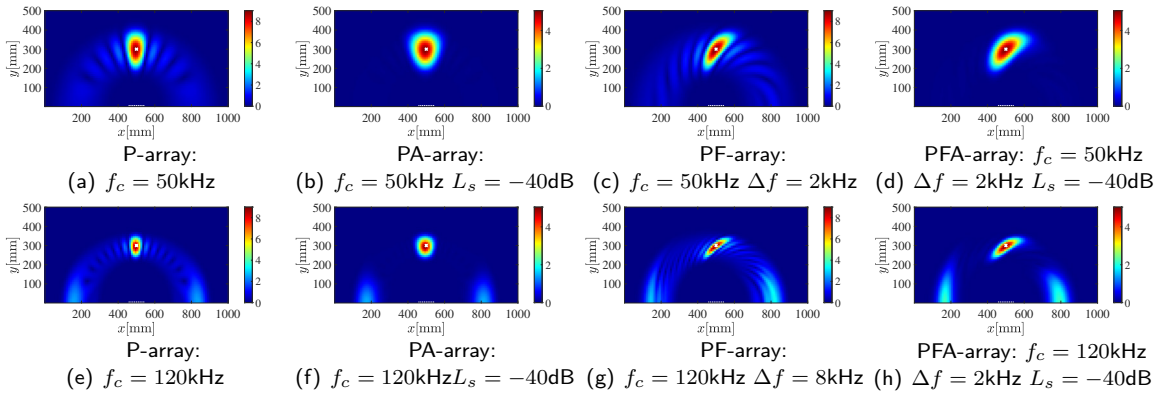

Fig. 2: The energy pattern focusing at (500,300) under 8-cycle tone burst with various arrays.

located at $(600, 250)$. In comparison, the PA-array demonstrates effective sidelobe suppression, as depicted in Figure 2(b,f) and Figure 3(b,f). However, this comes at the cost of an expanded main lobe width and enhanced grating lobe spot, as depicted in Figure 3(f).

For the PF-array, the shape of the focusing point is distorted, transitioning from a droplet-like form in P-array to an arc-like one in PF-array, as in Figure 2(c,g) and Figure 3(c,g). And the grating lobe spot is lowered and distracted, as in Figure 3(g).

The energy distribution for the PFA-array is presented in Figure 2(d,h) and Figure 3(d,h). While the combined control of amplitude and frequency offers enhanced flexibility, it may also introduce conflicting effects. As a result, the PFA-array does not always yield the optimal performance. A trade-off between sidelobe suppression and grating lobe mitigation is therefore necessary to achieve balanced array performance.

Experiments

The experiment is conducted on signal excitation and acquisition system which consists of waveform generator NI PXI-5412, piezo linear amplifier EPA-104, data acquisition card NI PXI-5122 with 8 acquisition channels and the monitor. The specimen is a T6061 aluminum alloy plate with the size of $1000 \times 1000 \times 2$ mm^3. The detailed parameters are listed as: density 2690 kg/m^3, Young's modulus 68.9 GPa and Poisson's ratio 0.33. The uniform linear array consists of 9 elements. The diameter and the thickness of the PZT wafer are 8 mm and 0.5 mm. The diagram of the experimental facilities and the aluminum plate are displayed in the Fig. 4. Two through-hole defects are thrilled at $D_1(500, 300)$,$D_2(600, 250)$ on the plate successively.

Results and Discussions

(1) P-array and PA-array

The excitation is set as the anti-dispersive 8-cycle tone burst centered at $f_c = 80$ kHz. The 6^{th} PZT is the transmitter and the others are receivers. The sidelobe attenuation level of the Chebyshev window is set as -40 in decibels (dB). The damage maps are displayed in the dB range of $[-130]$.

Figure 5 compares the damage from P-array and PA-array. In Fig. 5(a), the map from P-array exhibits several background noise artifacts, primarily caused by the presence of sidelobes. These sidelobes are effectively suppressed in the PA-array, as in Fig. 5(b), which shows a clean image without background noise artifacts. However, a drawback of introducing amplitude control is the broadening of the main lobe.

(2) P-array and PF-array

The excitation is set as the anti-dispersive 8-cycle tone burst. The 4^{th} element is the transmitter. The damage maps are displayed in the dB range of $[-10, 0]$. Figure 6 (a,c) and (b,d) compare the damage maps from P-array and PF-array, respectively.

Figure 6(a,b) show the result from P-array under center frequency $f_c = 50$ kHz and PF-array with the same center frequency and a frequency offset of $\Delta f = 2$ kHz. Compared to the shape of the damage spot in the damage map generated from the P-array in Figure 6(a), the damage spot from the PF-array appears distorted, as shown in Figure 6(b). Figure 6(c,d) compares the damage map under the tone burst excitation centered at $f_c = 120$ kHz with the frequency offset of $\Delta f = 8$ kHz. The damage spot is shrunk as the center frequency increases, as compared in Fig. 6(a,c). However, higher frequencies also increase the likelihood of grating lobe formation, which can introduce pseudo-damage. As shown in Figure 6(c), the P-array produces a pseudo-damage region near coordinates $(270, 160)$, attributed to the presence of a grating lobe. In contrast, Figure 6(d) illustrates that the PF-array effectively eliminates such pseudo-damage, demonstrating the suppression of grating lobes by appending the frequency control.

(3) PFA holo-array

Based on the above, side lobes and grating lobes

DOI 10.5162/Ultrasonic2025/C6-b3

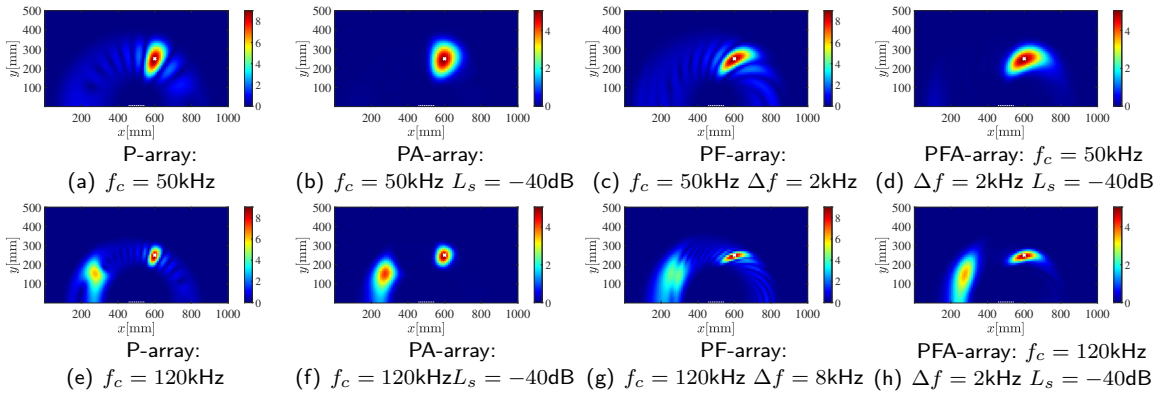

Fig. 3: The focusing energy pattern at (600,250) with the 8-cycle tone burst under various arrays.

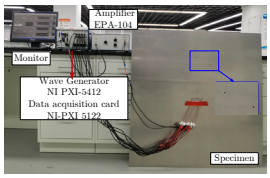

Fig. 4: The diagram of experiment set-up.

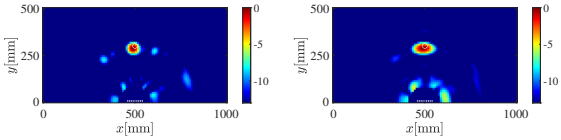

Fig. 5: The comparison of the damage map from (a) P-array and (b) PA-array.

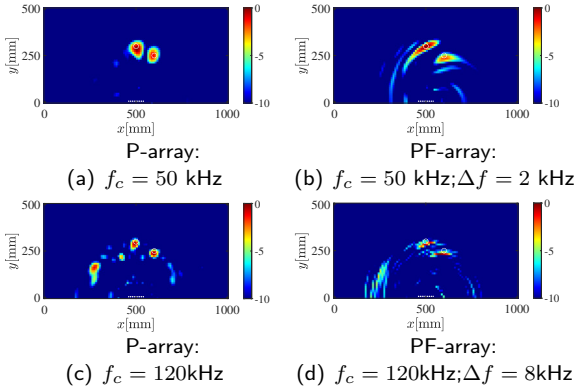

Fig. 6: The comparison of the damage map under (a,c) P-array (b,d) PF-array.

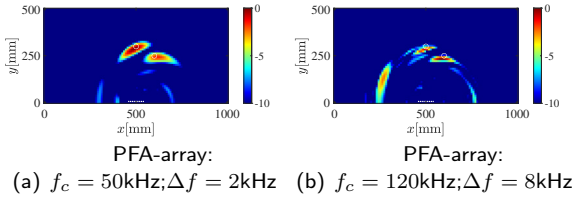

Fig. 7: The damage map under PFA-array under different excitations.

can be effectively suppressed in the PA-array and PF-array, respectively. In this section, damage maps for the PFA holo-array are displayed.

Figure 7 (a) and (b) exhibit the damage map from holo array under various tone burst excitation. It can be concluded that, when there is no grating lobes, the appending of the amplitude control helps to suppress the sides lobes. Compared with the damage map from PF-array in Figure 6(b), the background noise in Figure 7 (a) from the holo-array is reduced, but with the broadened damage spot width.

Nevertheless, in the presence of grating lobes, frequency control contributes to their suppression, whereas amplitude control tends to enhance the grating lobes while simultaneously reducing the side lobes. This behavior is illustrated in Figure 6(d) from PF-array, and in Figure 7(b) from the PFA holo-array.

Conclusions

Building upon the conventional P-array, where phase control is applied to individual array elements, this study further incorporates amplitude and frequency modulation into the array control strategy. Amplitude control effectively suppresses sidelobes but tends to broaden the main lobe and may exacerbate grating lobes. In contrast, frequency control helps reduce grating lobes. Simultaneously achieving a narrow main lobe, low sidelobes, and suppressed grating lobes is challenging; thus, a trade-off among these performance metrics is often required.

References

[1] L. Yu and V. Giurgiutiu. "In-situ optimized PWAS phased arrays for Lamb wave structural health monitoring". In: *Journal of mechanics of materials and structures* 2.3 (2007), pp. 459–487.

[2] P. Antonik et al. "Frequency diverse array radars". In: *2006 IEEE Conference on Radar*. IEEE. 2006, 3–pp.